J. Fluid Mech. (2005), *vol.* 543, *pp.* 267–292.
doi:10.1017/S002211200500652X Printed in the United Kingdom

On the resonant generation of large-amplitude internal solitary and solitary-like waves

By M. STASTNA† AND W. R. PELTIER

Department of Physics, University of Toronto, 60 St George Street, Toronto, ON M5S 1A7, Canada

(Received 23 April 2004 and in revised form 2 June 2005)

In this paper we discuss numerical simulations of the generation of large-amplitude solitary waves in a continuously stratified fluid by flow over isolated topography. We employ the fully nonlinear theory for internal solitary waves to classify the numerical results for mode-1 waves and compare with two classes of approximate theories, weakly nonlinear theory leading to the Korteweg–deVries and Gardner equations and conjugate flow theory which makes no approximation with respect to nonlinearity, but neglects dispersion entirely. We find that both weakly nonlinear theories have a limited range of applicability. In contrast, the conjugate flow theory predicts the nature of the limiting upstream propagating response (a dissipationless bore), successfully describes the bore's vertical structure, and gives a value of the inflow speed, c_j, above which no upstream propagating response is possible. The numerical experiments demonstrate the existence of a class of large-amplitude response structures that are generated and trapped over the topography when the inflow speed exceeds c_j. While similar in structure to fully nonlinear solitary waves, these trapped disturbances can induce isopycnal displacements more than 100 % larger than those induced by the limiting solitary wave while remaining laminar. We develop a theory to describe the vertical structure at the crest of these trapped disturbances and describe its range of validity. Finally, we turn to the generation of mode-2 solitary-like waves. Mode-2 waves cannot be truly solitary owing to the existence of a small mode-1 tail that radiates energy downstream from the wave. We demonstrate that, for stratifications dominated by a single pycnocline, mode-2 wave dissipation is dominated by wave breaking as opposed to mode-1 wave radiation. We propose a phenomenological criterion based on weakly nonlinear theory to test whether mode-2 wave generation is to be expected for a given stratification.

1. Introduction

The suggestion that vertically trapped solitary waves may exist in the interior of a density stratified fluid dates back to the early work of Benney (1966), who showed that an asymptotic expansion of the stratified non-rotating Euler equations in two parameters (an amplitude parameter and a parameter measuring the aspect ratio) yields the Korteweg–deVries (KdV) equation for the horizontal structure of the perturbations from a background state. The background state consists of a statically stable vertical density stratification profile, which provides the restoring force for the waves of interest, and (optionally) a horizontal background current. The

† Present address: Department of Applied Mathematics, University of Waterloo, 200 University Ave. West, Waterloo, ON N2L 3G1, Canada.

background shear flow, if any, is assumed to be linearly stable. It is well known that the KdV equation serves as the generic model of a nonlinear dispersive system in the long-wave limit, and hence allows solitary wave solutions that balance dispersion and nonlinearity (see, for example, Whitham 1974). Furthermore, a general initial condition evolves into a fixed number of rank-ordered solitary waves and a tail of small dispersive waves. Indeed, the initial-value problem for the KdV equation on an unbounded domain can be solved analytically by the celebrated method of inverse scattering (Whitham 1974), a truly remarkable property for a nonlinear equation.

Large-amplitude vertically trapped internal waves have been generated in the laboratory (Melville & Helfrich 1987; Grue *et al.* 2000) and observed in a number of locations in the ocean (Osborne & Burch 1980; Apel *et al.* 1985; Cummins *et al.* 2003). These have often been interpreted as internal solitary waves, though the physical situation, especially in the ocean, is generally quite complex and it is unlikely that the observed waves are true solitary waves in the language of a theorist. What is more, it has been shown (Lamb 1997) that large-amplitude internal solitary waves in a stratified fluid do not interact as solitary wave solutions of completely integrable equations, such as the KdV and Gardner equations, do, and hence are not solitons, according to the mathematical definition. Nevertheless, the observed waves are both stable and persistent and the theory, both weakly nonlinear (WNL) and exact, has provided a framework within which to discuss both experiment and observations.

In this paper, we present numerical simulations of the two-dimensional non-rotating Euler equations under the Boussinesq approximation demonstrating that the topographic or resonant generation mechanism is an efficient means for generating large-amplitude mode-1 internal solitary waves (ISWs). The generated waves are shown to match fully nonlinear ISWs, which are exact solutions of the full Euler equations. We discuss conditions under which the full range of ISW amplitudes predicted by the exact theory can be generated and provide a physical mechanism to explain cases in which this is not the case. Perhaps most importantly, we explicitly demonstrate the existence of a parameter regime in which the fluid response consists of extremely large, highly nonlinear, yet laminar, disturbances that are trapped over the topography. These trapped disturbances have a spatial structure that is similar to fully nonlinear ISWs of depression, but have an amplitude that is well above (more than double in certain cases) the limiting solitary wave amplitude. We develop a simple theory to describe the vertical structure at the crest of the trapped disturbances. This theory is based on the conjugate flow theory as discussed in Lamb & Wan (1998), for example, but has important mathematical differences that will be discussed in the following.

As weakly nonlinear theory dominates the interpretations of oceanographic measurements (Osborne & Burch 1980; Apel *et al.* 1985; Bougucki, Dickey & Redekopp 1997; Trevorrow 1998), we perform extensive comparisons of the results of our simulations with weakly nonlinear theory (WNL). We consider WNL for both freely propagating and topographically forced internal waves. For the former, we pay particular attention to the substantial literature on two-layer flow, as exemplified by the monograph of Baines (1995). In Baines (1995), it is argued that the Gardner equation yields structures that are qualitatively similar to those yielded by experiment. Unfortunately, the Gardner equation appears in the literature under a variety of names and in the following we will follow Baines in referring to it as the eKdV equation. The eKdV includes both a quadratic and cubic nonlinear term and exhibits solitary wave solutions that are bounded above by the limit of flat-centred waves (as opposed to breaking waves for the KdV equation). We find that while the eKdV equation provides a good qualitative description of the fluid response, for undisturbed interface heights located more than approximately 15 % of the total depth from the mid-depth, the

amplitude of the limiting solitary wave is significantly underestimated (in agreement with Baines 1995). The topographically forced weakly nonlinear theory based on the forced KdV, or fKdV, equation (Grimshaw & Smyth 1986) yields predictions on the range of inflow speeds that yield upstream propagating solitary waves. We find that the upper bound is incorrectly predicted by WNL, and that the nature of the error changes with the undisturbed interface height. The discrepancy between the simulations and WNL is explained using the conjugate flow theory, an alternative approximate theory that neglects dispersion altogether, but makes no approximation regarding nonlinearity. By its construction, conjugate flow theory is well-suited to the description of the central region of large-amplitude flat-centred waves.

The concept of topographic or resonant (hereinafter resonant only) generation of large upstream propagating internal waves was described by Grimshaw & Smyth (1986) who derived a forced KdV (fKdV) equation for the flow of a stratified fluid over broad small-amplitude isolated topography. The background current (labelled U) far upstream of the topography is specified to be independent of depth. The fKdV equation is not amenable to analytical techniques (such as the inverse scattering transform), consequently Grimshaw & Smyth (1986) integrated the fKdV equation numerically and found upstream propagating solitary waves for cases in which U lies in a band around the mode-1 (mode-n waves have isopycnal deflections that cross zero $n-1$ times in the interior of the fluid), linear longwave speed. Physically, we imagine that the flow over the topography generates both upstream and downstream propagating linear, vertically trapped waves. However, when the difference between U and the mode-1, linear long-wave speed is small, the upstream propagation is retarded or precluded altogether. The waves thus remain in the forcing region longer, and grow in amplitude. The growth continues until the waves reach a sufficient amplitude to move upstream (both weakly nonlinear and fully nonlinear theory predict that larger waves have larger propagation speeds) and away from the topography.

The literature concerning the weakly nonlinear theory of resonant generation is voluminous. Recent examples include the work of Porter & Smyth (2002) that discusses resonant generation in the context of atmospheric ISWs, namely the morning glory clouds observed near the Gulf of Carpentaria, and the work of Wang & Redekopp (2001) that derives a model equation allowing for time-dependent background currents and discusses possible instabilities induced in the bottom boundary layer by resonantly generated ISWs. The reader is referred to these papers and the references therein for a more complete bibliography.

A notable shortcoming of weakly nonlinear theories is the lack of a clear upper bound (in terms of wave amplitude) on their range of applicability. The finite-amplitude theory of Grimshaw & Zengxin (1991) for a linearly stratified fluid, which is not weakly nonlinear, but employs the formalism of the weakly nonlinear theory found in Grimshaw & Smyth (1986) as well as the assumption of a separable solution, includes a criterion for the onset of overturning, and as such formally describes the full range of ISW amplitudes. However, the separable (in space) description necessarily breaks down at the onset of wave breaking and as the theory depends crucially on the assumption of a constant N^2, the utility of this theory for cases with more general stratification profiles is unclear.

The weakly nonlinear theory, as presented in Grimshaw & Smyth (1986), makes no distinction between mode-1 waves and higher-mode waves. Thus, in principle, resonant generation of mode-2 solitary waves should simply require matching U to the mode-2, linear long-wave speed. However, it has been shown by Akylas & Grimshaw (1992) that solitary waves of mode-2 or higher develop oscillatory tails (of lower mode than the main solitary wave body). As the group speed of the dispersive

waves that make up the tail is smaller than their phase speed, these tails can radiate energy from the main wave and hence higher mode waves are not truly solitary. This means that the exact theory for mode-1 ISWs has no analogue for higher-mode waves and we discuss, with an example, the possibility of resonantly generating mode-2 waves and the physical processes leading to wave decay. In particular, we demonstrate that for a stratification dominated by a single pycnocline, the damping of mode-2 solitary-like waves owing to wave radiation is small when compared to the changes of wave shape owing to wave breaking.

Experimental studies of mode-2 solitary-like waves date back to the work of Davis & Acrivos (1967). Aspects of the generation, propagation, collisions (wave–wave and wave–wall), and wave decay due to viscous effects of mode-2 waves have been the subject of recent experimental studies (Stamp & Jacka 1996; Schmidt & Spigel 2000; Mehta, Sutherland & Kyba 2002). A trailing mode-1 tail is a robust feature of the experiments, as are regions of overturned isopycnals and localized turbulence. However, the numerical simulations of mode-2 waves reported in the literature (Terez & Knio (1998) for unsteady waves; Tung, Chan & Kubota (1982) for steady waves) actually consider mode-1 waves only. Both sets of authors argue that once mode-1 waves are computed, the stratification can be extended in a symmetric manner and mode-2 waves recovered (the figures in both papers are produced in this manner). While this technique is computationally efficient (the vertical extent of the domain is halved), it precludes any consideration of the interaction of mode-2 waves with small-amplitude mode-1 tails. The resonantly generated mode-2 waves in our simulations have no obvious horizontal lines of symmetry, and this casts some doubt on the direct relevance to mode-2 solitary-like waves of simulations of mode-1 ISWs. We proceed to develop a phenomenological criterion based on weakly nonlinear (KdV) theory to assess whether, given stratification and background current profiles, we would expect mode-2 waves to be efficiently generated.

In summary, § 2 outlines the theoretical and computational background, § 3 discusses the generation of mode-1 ISWs and large trapped disturbances, § 4 compares the present study with previous work on the flow of two-layer fluids over isolated topography and especially the weakly nonlinear theories employed to interpret experiments, § 5 addresses the issue of whether resonantly generated mode-2 solitary-like waves are dominated by wave breaking or a mode-1 tail, and § 6 summarizes the results. Also in § 6, we discuss the applicability of our simulations to laboratory experiments and comment on several avenues for future work.

2. Descriptions of ISWs

We consider a non-rotating incompressible inviscid fluid under the Boussinesq approximation. In a fixed frame of reference with the origin at the ocean floor, the x-axis parallel to the flat ocean bottom and the z-axis pointing upward ($\hat{k}$ is the upward pointing unit vector) the governing equations read,

$$\frac{\partial \boldsymbol{u}}{\partial t} + \boldsymbol{u}\cdot\nabla\boldsymbol{u} = -\nabla P - \rho g\hat{\boldsymbol{k}} + \boldsymbol{F}_b, \tag{2.1}$$

$$\nabla\cdot\boldsymbol{u} = 0, \tag{2.2}$$

$$\frac{\partial \rho}{\partial t} + \boldsymbol{u}\cdot\nabla\rho = 0, \tag{2.3}$$

where we have divided the momentum equations (2.1) by the constant reference density ρ_0 (and absorbed the constant into the pressure, P, as is conventional). In (2.1), we

include the non-standard term $\boldsymbol{F}_b$. This body force (technically an acceleration) term may be employed to set the fluid in motion over topography in numerical simulations, and is included only in the numerical formulation of the problem. Throughout, we assume that a rigid lid exists at $z = H$ and that the fluid motion is two-dimensional.

In order to describe ISWs theoretically, we employ the incompressibility of the fluid to introduce a streamfunction $\psi(x, z, t)$ so that $(u, w) = (\psi_z, -\psi_x)$ where subscripts denote partial derivatives. For the moment, we assume that there is no background current. The extension to the case of a background shear flow, $U(z)$, is discussed by Benney (1966) and Stastna & Lamb (2002), among others. To maintain consistency with Benney (1966) and Stastna & Lamb (2002), we introduce the buoyancy $b = -g\rho = -g(\bar{\rho}(z) + \rho'(x, z, t))$, where $\bar{\rho}(z)$ is the background density or stratification profile, which we assume to be statically stable. Linearizing and assuming a vertically trapped form for the disturbance, i.e. $\psi = a_0 \exp(\mathrm{i}k(x - ct))\varphi(z)$, we find that $\varphi(z)$ is governed by the eigenvalue problem

$$\varphi_{zz} + \left(\frac{N^2(z)}{c_l^2} - k^2\right)\varphi = 0, \tag{2.4}$$

$$\varphi(0) = \varphi(H) = 0, \tag{2.5}$$

where

$$N^2(z) = -g\frac{\mathrm{d}\bar{\rho}(z)}{\mathrm{d}z}, \tag{2.6}$$

is the definition of the buoyancy frequency squared (recall we have already scaled out ρ_0). The buoyancy frequency gives the frequency of oscillation of a fluid parcel infinitesimally displaced from a state of rest at height z. For a statically unstable fluid, $N^2 < 0$ somewhere in the fluid.

For a general stratification profile, (2.4), (2.5) must be solved numerically. No generality is lost by focusing on rightward propagating waves, and we shall hereinafter do so. In the absence of a background shear current, leftward propagating waves are trivial to recover. In general it is found, and can be proved rigorously (see for example, Yih 1965), that the propagation speed c_l decreases both as the mode number increases, and as wavelength decreases. Thus, mode-1 long waves ($k = 0$) propagate faster than any other vertically trapped linear waves. This, however, is not true for higher-mode long waves (mode-2 in particular), and it is possible that mode-2 long waves propagate at the same speed as shorter mode-1 waves. In the following, mode-n propagation speeds and eigenfunctions in the long-wave limit will be denoted as $c_{lw}^{(n)}$ and $\phi^{(n)}(z)$, respectively, where the governing eigenvalue problem reads

$$\phi_{zz} + \frac{N^2(z)}{c_{lw}^2}\phi = 0, \tag{2.7}$$

$$\phi(0) = \phi(H) = 0. \tag{2.8}$$

As mode-1 ISWs are exceptional, the superscript 1 will be suppressed.

Weakly nonlinear long-wave theory for ISWs (see Benney 1966 or Lamb & Yan 1996 for details) yields, at leading order

$$\psi = \sum_{n=1}^{\infty} c_{lw}^{(n)} B^{(n)}(x, t)\phi^{(n)}(z), \tag{2.9}$$

$$b = \sum_{n=1}^{\infty} N^2(z) B^{(n)}(x, t)\phi^{(n)}(z). \tag{2.10}$$

However, the shape of the horizontal structure is undetermined at leading order. We concentrate on mode-1 waves and hence drop all other modes from consideration for the time being. To first-order in the nonlinearity and dispersion parameters, B is governed by the Korteweg–de Vries (KdV) equation

$$B_t = -c_{lw} B_x + 2 r_{10} c_{lw} B B_x + r_{01} B_{xxx}. \tag{2.11}$$

The solitary wave solutions of this equation are given by

$$B(x,t) = -b_0 \mathrm{sech}^2(\theta), \tag{2.12}$$

$$\theta = \frac{x - Vt}{\lambda}, \tag{2.13}$$

$$V = c_{lw}\left(1 + \tfrac{2}{3} r_{10} b_0\right), \tag{2.14}$$

$$b_0 \lambda^2 = -6 \frac{r_{01}}{c_{lw} r_{10}}. \tag{2.15}$$

It can be seen that the solitary wave properties (propagation speed, half-width) depend not only on the wave amplitude b_0, but also the so-called nonlinearity (r_{10}) and dispersion (r_{01}) parameters. These are given by

$$S = \int_0^H (\phi'(z))^2 \, \mathrm{d}z, \tag{2.16}$$

$$r_{10} = -\frac{3}{4} \frac{\int_0^H (\phi'(z))^3 \, \mathrm{d}z}{S}, \tag{2.17}$$

$$r_{01} = -\tfrac{1}{2} c_{lw} \frac{\int_0^H (\phi(z))^2 \, \mathrm{d}z}{S}, \tag{2.18}$$

and as such have a non-trivial dependence on the density stratification (via the eigenvalue problem (2.7), (2.8)). Since $r_{01} < 0$, the linear dispersion relation of (2.11) demonstrates that longer waves travel faster. In contrast to r_{01}, r_{10} can take on either sign. By demanding that λ is real, we find $r_{10} b_0 > 0$ and hence from (2.14) that larger-amplitude solitary waves travel faster.

If we define the onset of wave breaking as the point at which a streamline, in a frame moving with the wave, becomes vertical (i.e. $\psi_z = 0$), then the KdV theory allows us to find an expression for the breaking amplitude. In the frame moving with the wave, we have $\psi = -Vz + c_{lw} B(x,t) \phi(z)$. Demanding that $\psi_z = 0$ and using the definition of V (2.14), we find that at the onset of breaking

$$1 = -b_0\left(\tfrac{2}{3} r_{10} + \phi'(z)\right). \tag{2.19}$$

for some value of z. Of course, this value is not expected to be quantitatively accurate since breaking is a finite-amplitude phenomenon and a more accurate prediction is given by fully nonlinear theory as described below.

Finally, if we consider the displacement of an isopycnal passing through the point (x, z) from its rest height (labelled η), we find that KdV theory gives the expression

$$\eta^{WNL} = B(x,t)\phi(z), \tag{2.20}$$

where the superscript WNL denotes a quantity given by weakly nonlinear theory.

The fully nonlinear theory for ISWs is generally written in terms of the isopycnal displacement, $\eta(x,z)$. In the following, we will identify the maximum isopycnal displacement with the wave amplitude and label it η_{max}. Fully nonlinear, rightward

propagating ISWs in a frame moving with the wave speed are governed by a nonlinear elliptic eigenvalue problem, namely the Dubreil–Jacotin–Long (DJL) equation

$$\nabla^2\eta + \frac{N^2(z-\eta)}{c^2}\eta = 0, \tag{2.21}$$

$$\eta = 0 \quad \text{at } z = 0, H, \tag{2.22}$$

$$\eta = 0 \quad \text{as } |x| \longrightarrow \infty, \tag{2.23}$$

where the propagation speed c is to be determined as part of the solution. Once η and c are known, the wave-induced velocities are computed from the relation $\psi = c\eta$. To the best of our knowledge, there are no explicit solutions of the DJL equation when N^2 is not constant. The direct variational method due to Turkington, Eydeland & Wang (1991), which is a component of a rigorous proof of the existence of fully nonlinear ISWs, has been successfully implemented in several studies of fully nonlinear ISWs (i.e. Lamb & Wan 1998; Stastna & Lamb 2002; Stastna & Peltier 2004), and will be used throughout this article to compute fully nonlinear ISWs. In Stastna & Lamb (2002), the processes that provide the upper bound on possible solitary wave amplitudes for any one stratification–background current combination are classified into three categories.

(i) Streamline overturning and the formation of a trapped, recirculating core, which we label the breaking limit.

(ii) Shear instability of the wave-induced currents, which we label the instability limit.

(iii) Wave broadening to a limiting flat-centred wave, which we label the conjugate flow limit.

All cases discussed here have ISW amplitude bounded above by the conjugate flow limit.

We note briefly that the direct variational solution technique fixes the available potential energy for the ISW *a priori* and minimizes the perturbation kinetic energy in the space of disturbances satisfying the boundary conditions. This means that neither the wave amplitude nor the propagation speed are fixed *a priori*, this is especially convenient in computing broad flat-centred ISWs.

Note that the essential difference between the DJL equation and the equation governing the vertical structure of linear long waves (2.7) is that in the DJL equation the buoyancy frequency squared is evaluated at the undisturbed isopycnal height $(z - \eta(x, z))$. By demanding an isopycnal displacement that is independent of x (an excellent approximation in the central region of broad flat-centred waves) we find that the DJL equation reduces to the nonlinear ordinary differential eigenvalue problem that governs conjugate flows (Lamb & Wan 1998). The solution of the nonlinear conjugate flow eigenvalue problem requires an auxiliary condition, which may be interpreted as the conservation of momentum flux (Lamb & Wan 1998). In order to determine the fully nonlinear waveform, however, the dispersion due to finite wavelength (the η_{xx} term in the DJL equation) is essential. In all cases in which a single stable mode-1 conjugate flow exists, the conjugate flow speed, which we label c_j, and maximum isopycnal displacement, which we label η_j, provide the upper bound on ISW propagation speed and amplitude, respectively. We note briefly that higher-mode conjugate flow solutions also exist, though their significance as an upper bound to ISW amplitude is unclear (Rusas & Grue 2002).

For the time-dependent simulations of the resonant generation process, the field equations (2.1)–(2.3) are solved using a variable time step second-order projection

technique described in Lamb (1994) and Bell & Marcus (1992). Briefly, the model employs terrain following coordinates, imposes a no-flux boundary condition at the bottom ($z = g(x)$ with $g(x)$ specified below) and top, and allows the free propagation of non-hydrostatic waves through the vertical right-hand boundary. At the left-hand boundary, the influx of fluid is specified (hence, ISWs reflect from the left-hand boundary and we terminate all simulations before this occurs). There is no damping, sponge layer, or diffusion (save for the negligible amount due to discretization) in the model. While certain applications (e.g. sediment resuspension) require the accurate representation of the viscous bottom boundary layer, the model itself is stable with no viscosity by virtue of its construction and provides an accurate representation of the fluid flow unless three-dimensionality of the flow becomes dominant.

We will present the results of our numerical simulations in non-dimensional form. Towards this end we choose H, the height of the domain, as a typical length scale, c_{lw}, the mode-1 linear long-wave speed as a characteristic velocity, and the advective time scale $T = H/c_{lw}$ as a characteristic time scale.

The shape of the small-amplitude topography employed is given by

$$g(x) = h \ \mathrm{sech}\left(\frac{x}{a}\right), \tag{2.24}$$

where h and a determine the height and width of the topography. We will refer to cases with $h > 0$ (< 0) as positive (negative) topography.

Throughout the majority of this paper we will employ a generic stratification for both a model coastal ocean and a laboratory set-up aiming to model the coastal ocean. The stratification employed consists of an essentially unstratified mixed layer adjacent to the upper boundary, a strong subsurface pycnocline located one-fifth of the water depth below the surface, and a weakly stratified layer below the main pycnocline. We choose to specify $N^2(z)$, the buoyancy frequency squared, using the analytic expression:

$$T^2N^2(z) = (p-q)\mathrm{sech}^2\left(\frac{z-z_0}{d}\right) + \frac{q}{2}\left[1 - \tanh\left(\frac{z-z_0}{d}\right)\right]. \tag{2.25}$$

This allows us to identify $p - 0.5q$ with the strength of stratification in the main pycnocline and q with the strength of stratification in the deep. Throughout this paper, we set $p = 63.1$ and $q = 3.156$. With this choice of parameters the maximum of N^2 is a factor of twenty larger than N^2 at the model ocean bottom, a reasonable, though non-unique choice for the coastal ocean.

The parameters z_0 and d specify the centre and thickness of the main pycnocline, respectively. All of the simulations discussed in this paper fix $d = 0.05$. Simulations involving mode-1 ISWs set $z_0 = 0.8$. For this choice of stratification, both the amplitude and propagation speed of the the exact ISW solutions are bounded above by the conjugate flow limit.

Simulations involving mode-2 waves set $z_0 = 0.55$. For all stratifications considered, ISWs can have a single polarity only, and at most a single stable mode-1 conjugate flow exists. See Lamb & Wan (1998) for a discussion of stratifications for which ISWs of depression and elevation are possible. An expression for the density profile corresponding to (2.25) (which we employ as an initial condition for the density) can be derived either numerically or analytically from the definition of buoyancy frequency (2.6). As both the horizontal and vertical velocities are initially taken to vanish, we require a mechanism for setting the fluid in motion. This may be accomplished by one of two methods. The first defines a fictitious acceleration on the time interval

$0 < t < T_f$, of the form:

$$\boldsymbol{F}_b = \left[\frac{U}{T_f}\left(1 - \cos\left(\frac{2\pi t}{T_f}\right)\right), 0\right], \tag{2.26}$$

where U is the desired value of the horizontal velocity far upstream, and T_f is the time period of the forcing. The forcing is assumed to vanish for $t > T_f$. The second uses a similar functional form, but specifies the rate of change of the horizontal velocity at the left-hand boundary.

The merits of the first method are discussed in Stastna & Peltier (2004), though the latter proves somewhat easier to implement in the numerical model. We have found that the two methods yield identical results. For an essentially impulsive start, employed throughout the majority of this paper, unless otherwise noted, we set $T_f = 0.035$. The combinations of parameters (U, T_f, h, a) and (U, h, a) will be referred to in the following as the forcing parameters. If T_f is suppressed, it is set to $T_f = 0.035$.

Several different resolutions were employed for the simulations discussed in the following section. In all cases, we have ensured that the results presented are not influenced by resolution doubling. For all non-breaking mode-1 waves, a vertical resolution of 0.01 and a horizontal resolution of 0.04 proved sufficient, though all figures in the following are based on simulations with a resolution of 0.01 by 0.01. For breaking waves, resolution becomes an issue only after the onset of overturning. However, at this point in the simulation, three-dimensional effects, neglected in our study, are expected to play a significant, and perhaps dominant, role. Because of possible resonance with shorter mode-1 waves (discussed below), the resonant generation of mode-2 waves required a finer horizontal resolution. For the cases discussed in the text, we employed a horizontal resolution of 0.005 and a vertical resolution of 0.005.

3. Generation of mode-1 ISWs

The resonant generation process is illustrated in figure 1 for stratification (2.25) with $(z_0, d) = (0.8, 0.05)$ and forcing parameters $(U, h, a) = (0.9, 0.1, 1)$. For reference, $c_j = 1.25$. Figure 1(a) shows the shaded density contours in a portion of the computational domain at $t = 135.0$. The leading upstream (leftward) propagating ISW is well upstream of the topography (the white hill in this case). The crest of the leading ISW ($\eta_{max} \approx 0.11$ or about 35 % of the conjugate flow amplitude and $c \approx 0.91 c_j$) is indicated by a vertical black line. In figure 1(b), we show the vertical profile of the wave-induced horizontal velocity at the leading ISW crest extracted from the simulation, along with two theoretical profiles. The profile of the fully nonlinear waves is computed using the variational method described in the previous section, while the wave amplitude in the case of weakly nonlinear theory is chosen so that the horizontal velocity matches at the surface. It is clear from figure 1(b) that the velocity profile predicted by the fully nonlinear theory matches that extracted from the simulation essentially exactly. A similar match between ISWs yielded by the simulations and fully nonlinear theory was found regardless of ISW amplitude, from the smallest tried, up to the conjugate flow limit. The weakly nonlinear theory, on the other hand, gives at best a qualitative approximation. This is especially true since we 'tuned' the wave amplitude in the weakly nonlinear theory to match the vertical profile of wave-induced horizontal velocity. For the same estimate of amplitude, the weakly nonlinear prediction of the wave-induced horizontal velocity (the horizontal

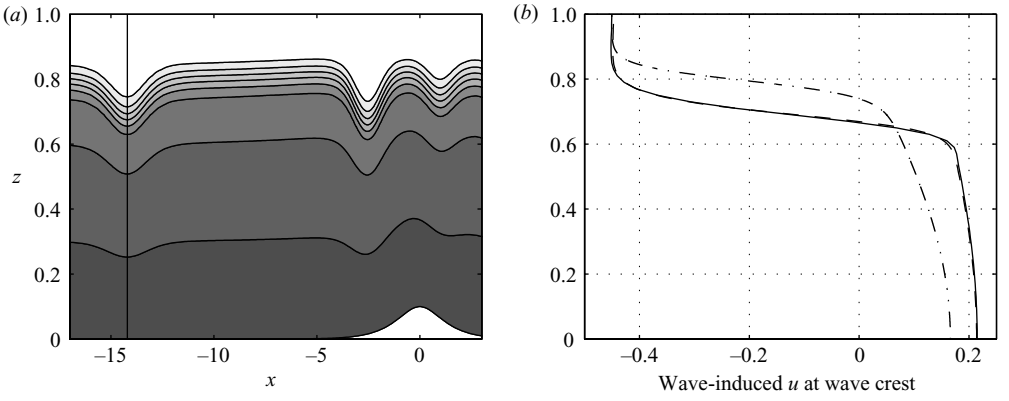

FIGURE 1. $(U, h, a) = (0.9, 0.1, 1)$. (a) Shaded density contours. The crest of the leading upstream propagating ISW is shown by a vertical black line. (b) Wave-induced horizontal velocity at the wave crest. —, simulation; - - -, fully nonlinear theory –·–, leading-order weakly nonlinear theory with the wave amplitude chosen so that the wave-induced horizontal velocity at the surface matches the simulation values.

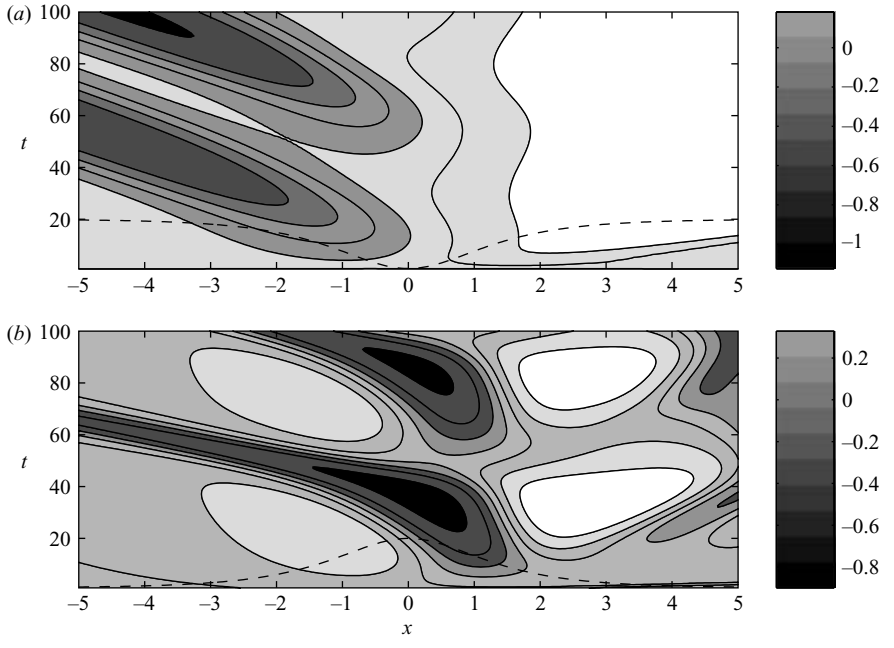

FIGURE 2. Hovmöller plots of the wave-induced horizontal velocity at the surface $(z = 1)$. The shape of the topography is indicated by a black dashed lined. (a) $(U, h, a) = (1.12, -0.1, 1)$, (b) $(U, h, a) = (0.9, 0.1, 1)$. Note that the ISWs are generated over the downsloping portion of the topography.

structure is given by the solitary wave solution of the KdV equation, (2.12)) at the bottom would be very poor. In figure 1(a), a second ISW is propagating down the upstream slope of the topography, while a third is forming on the downstream slope. That the ISWs of depression form on the downstream slope is confirmed in figure 2 in which we show Hovmöller (space–time) plots of the wave-induced horizontal velocity

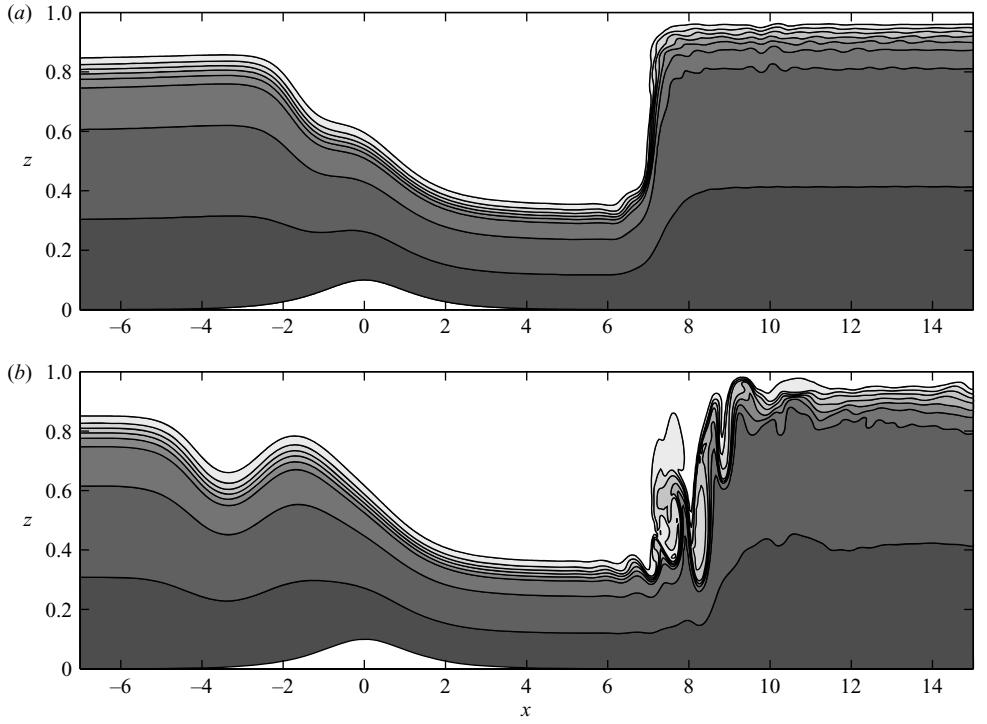

FIGURE 3. Shaded density contours $(U, h, a) = (0.955, 0.1, 1)$. (*a*) $t = 106.8$, (*b*) $t = 121$. Note the large response downstream that appears to undergo shear instability while the upstream response is very similar to figures 1(*a*) and 2(*a*).

at the surface ($z = 1$). The upstream propagating waves appear as dark streaks of negative velocity that slope up and to the left. For illustrative purposes, the shape of the topography is indicated by a dashed line. The case shown in figure 2(*a*) has the forcing parameters $(U, h, a) = (1.12, -0.1, 1)$. In this case, the upstream propagating ISWs are larger ($\eta_{max} \approx 0.26$ or about 85 % of the conjugate flow amplitude). The response downstream of the topography, consists of a long wave of elevation that permanently raises the pycnocline downstream of the topography, but otherwise does not interfere with the ISW generation process. It can be noted that the second upstream propagating ISW is about 7 % larger than the first.

For the case of positive topography, the downstream response can be complex, as is evident from figure 2(*b*). Indeed, a minor modification of the forcing conditions, $(U, h, a) = (0.955, 0.1, 1)$, while leaving the upstream response largely unaffected, leads to the formation of a large-amplitude bore on the downstream side of the topography. The shaded density contours in the vicinity of the topography are shown in figure 3. The response downstream of the topography consists of a region of depressed isopycnals followed by a steep face that raises the isopycnals well above their far upstream, or undisturbed, positions. Beyond the steep face, the isopycnals slope downward extremely slowly. The bore terminates well outside of the portion of the computational domain shown. In figure 3(*a*) ($t = 106.8$), we can see that the steep face and slowly downsloping isopycnals undergo what appears to be a shear instability. Regions of overturning form rapidly and billows are clearly visible by $t = 121$ (figure 3(*b*)).

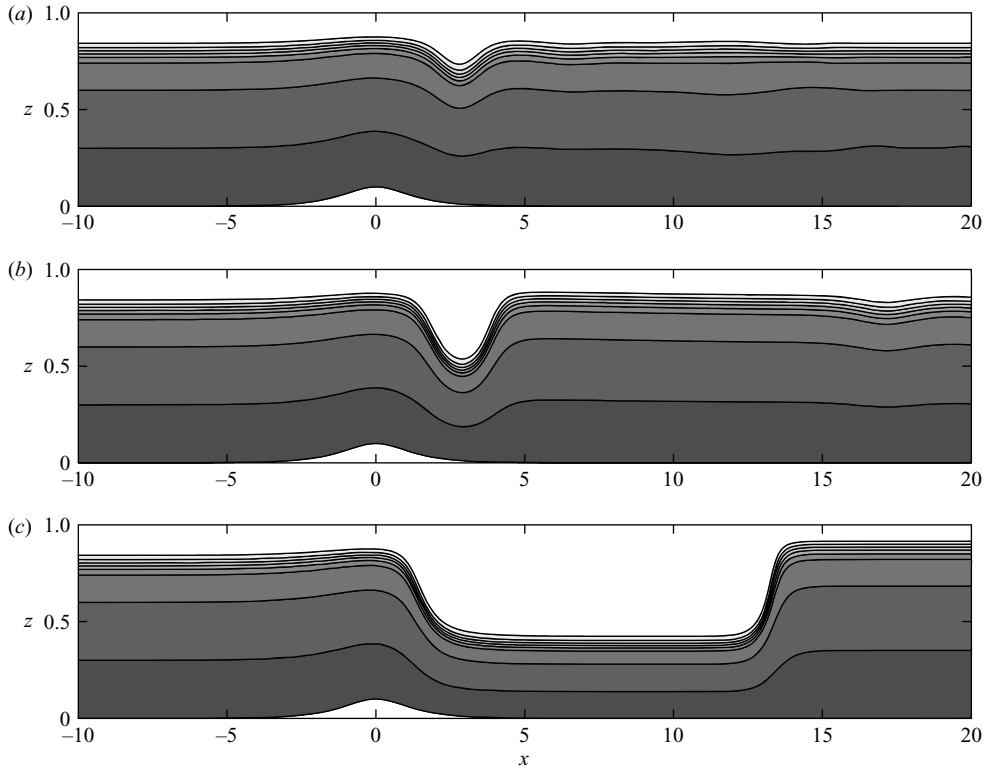

FIGURE 4. Shaded density contours $(U, h, a) = (1.12, 0.1, 1)$. (a) $t = 17.8$, (b) $t = 71.2$, (c) $t = 213.7$. While the value of U far upstream is below c_j, the depth-averaged horizontal velocity at the crest of the topography exceeds c_j resulting in wave blocking and no upstream ISW propagation. The growing lee wave is upstream directed.

The vertically averaged horizontal velocity of the fluid increases over the crest of the positive topography above its far upstream value. Since upstream propagating ISWs are generated on the downstream slope of positive topography, beyond $U = (1 - h(0))\, c_j$ the wave generated on the downstream slope cannot propagate over the crest of the topography and upstream. In figure 4, we show shaded density contours for a simulation with the forcing parameters $(U, h, a) = (1.12, 0.1, 1)$. Figures 4($a$), 4($b$) and 4($c$) show the wave evolution at $t = 17.8$, 71.2 and 213.7, respectively. The wave of depression on the downstream slope of the topography connects to the elevated isopycnals over the topography and terminates with a second region of elevated isopycnals and a tail of small ISWs and other dispersive waves that are swept downstream by the background current. As the wave of depression over the downstream slope increases in amplitude, the downstream region of elevated isopycnals grows in amplitude and horizontal extent. For long times, the wave of depression over the downstream slope tends to a flat-centred wave with an amplitude that is larger than the conjugate flow amplitude (about 135 % of the conjugate flow amplitude). Crucially, however, it is followed by a downstream region of elevated isopycnals. Neither of these states is conjugate to the region far upstream of the topography, though they appear to be conjugate to one another. In principle, a series of conjugate flow calculations (including shear background currents as necessary) could be carried out to connect the three states, though this has not been carried out here.

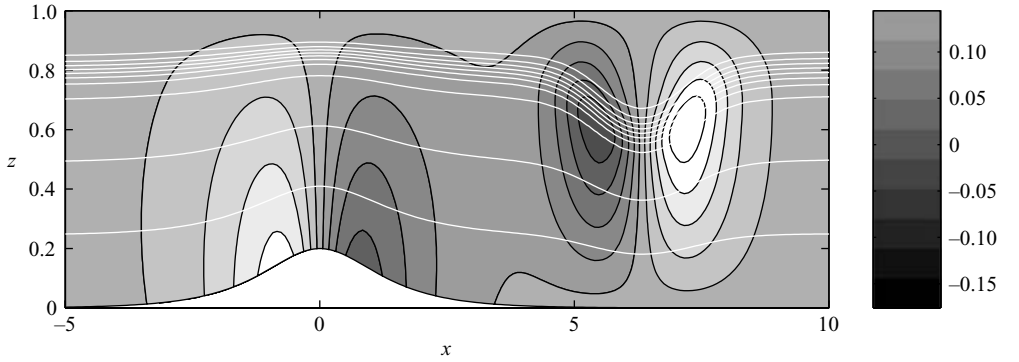

FIGURE 5. Shaded vertical velocity contours. Density contours are given by superimposed white lines. $(U, h, a) = (1.236, 0.2, 1)$. The structure of the wave-induced vertical currents indicates that the wave is upstream directed, $(\eta_{max}, c) = (0.195, -1.208)$. However, as $U > -c$, the wave is swept downstream, yet retains its solitary character.

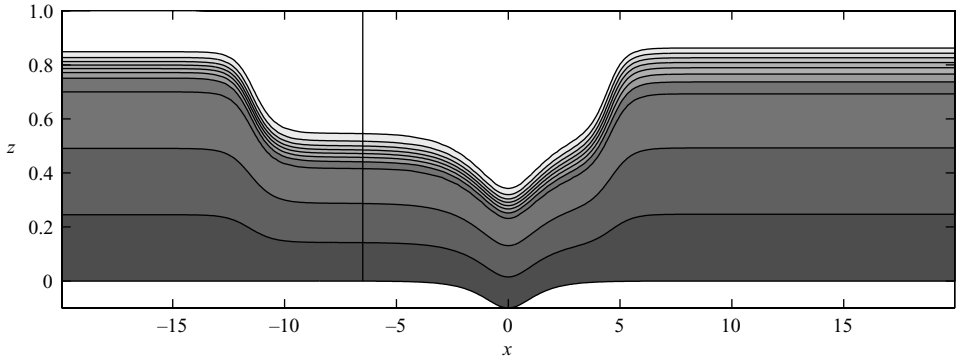

FIGURE 6. Shaded density contours for a slow moving, dissipationless bore as it propagates upstream. $(U, h, a) = (1.236, -0.1, 1)$ or $U = 0.99c_j$. The vertical black line denotes the region in which the wave-induced isopycnal displacement and horizontal velocity are given by the solution to the conjugate flow eigenvalue problem.

As U is increased further, the waves formed on the downstream slope remain on the downstream slope (the forcing region) for a shorter amount of time before being swept downstream by the background current. In figure 5, we show the shaded vertical velocity contours for a simulation with forcing parameters $(U, h, a) = (1.236, 0.2, 1)$. Superimposed on the shaded vertical velocity contours are white density contours. Downstream of the topography, we see an ISW of depression ($\eta_{max} \approx 0.195$). The geometrical distribution of the velocity contours indicates that, in a stationary fluid, the wave would be upstream propagating.

For the cases with negative topography, the flow evolution exhibits consistent characteristics for a broad range of U values. With $h = -0.1$, upstream propagating ISWs are clearly visible for $U > 0.88$ and increase in amplitude as U increases. ISWs become noticeably broader once $U > 1.15$ and when $U = 1.236 = 0.99c_j$, the upstream propagating wave takes the form of a slow-moving dissipationless bore. The shaded density contours are shown in figure 6. The vertical black line denotes the approximate region in which the wave-induced horizontal velocity and isopycnal profiles match those found by solving the eigenvalue problem governing conjugate flows, as well as solutions of the DJL equation for a flat-centred ISW.

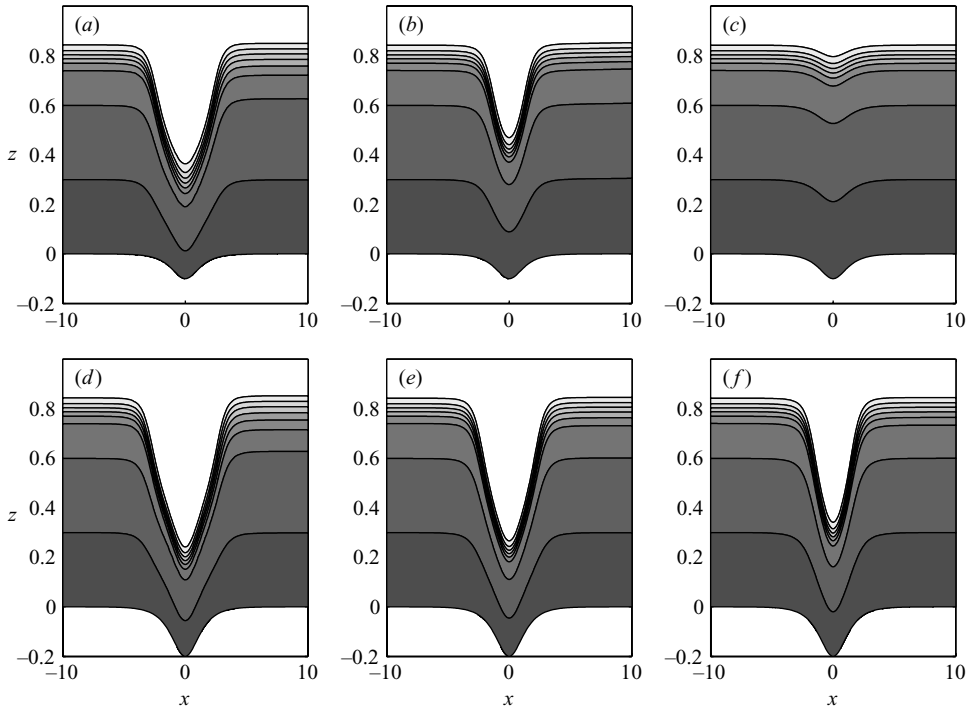

FIGURE 7. Shaded density contours for various trapped disturbances. The amplitude of the topography is fixed at $h = -0.1$ and -0.2 for (a)–(c) and (d)–(f), respectively. The upstream velocity and approximate disturbance amplitude are: (a) $U = 1.35 = 1.08c_j$, $\eta_{max} \approx 0.5$, (b) $U = 1.4 = 1.12c_j$, $\eta_{max} \approx 0.38$, (c) $U = 1.52 = 1.22c_j$, $\eta_{max} \approx 0.06$, (d) $U = 1.35 = 1.08c_j$, $\eta_{max} \approx 0.62$, (e) $U = 1.4 = 1.12c_j$, $\eta_{max} \approx 0.59$, (f) $U = 1.52 = 1.22c_j$, $\eta_{max} \approx 0.52$.

Once U exceeds c_j, no upstream-propagating waves are possible upstream of the topography. However, over the negative topography, the background current is reduced and thus localized disturbances may form. We expect these to be trapped over the topography as any disturbances that drift downstream of the topography are rapidly swept downstream and out of the computational domain. In figure 7, we show the shaded density contours for a variety of forcing cases. The topography width is fixed ($a = 1$) for all cases shown. The amplitude of the topography is fixed at $h = -0.1$ and -0.2 for figures 7(a)–7(c) and 7(d)–7(f), respectively. The upstream velocity and approximate disturbance amplitude are: (a) $U = 1.35 = 1.08c_j$, $\eta_{max} \approx 0.5$, (b) $U = 1.4 = 1.12c_j$, $\eta_{max} \approx 0.38$, (c) $U = 1.52 = 1.22c_j$, $\eta_{max} \approx 0.06$, (d) $U = 1.35 = 1.08c_j$, $\eta_{max} \approx 0.62$, (e) $U = 1.4 = 1.12c_j$, $\eta_{max} \approx 0.59$, (f) $U = 1.52 = 1.22c_j$, $\eta_{max} \approx 0.52$. The extremely large amplitude and apparent stability of the trapped disturbances are surprising. We have confirmed that the disturbance-induced currents are qualitatively similar to those induced by an upstream propagating ISW of depression. The analogy with ISWs is not exact, as the disturbance amplitude decreases as U (and hence the putative disturbance propagation speed) increases. It should also be noted that the exact shape of the topography is unimportant and trapped disturbances that are more complex than a single hump (i.e. a double hump) are easily generated by an appropriate choice of bottom topography.

While a solution procedure for the DJL equation with a fixed value of c and the bottom boundary condition $\eta(x, g(x)) = g(x)$ is unavailable for a general $N^2(z)$

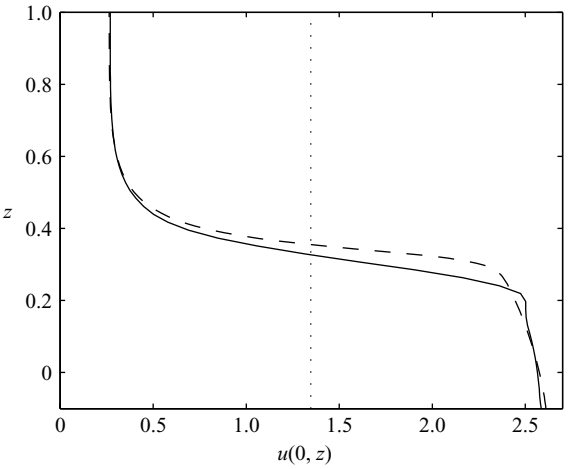

FIGURE 8. Disturbance-induced horizontal velocity at the topography crest. —, figure 7(*b*); - - -, predictions of (3.1)–(3.3) with $h = -0.1$ and $U = 1.4. \ldots, U$.

profile (though see Laprise & Peltier (1988) for the constant N^2 case), the conjugate flow eigenvalue problem may be easily converted to a two-point ordinary differential boundary-value problem,

$$\eta_{zz} + \frac{N^2(z-\eta)}{U^2}\eta = 0, \tag{3.1}$$

$$\eta(h) = h, \tag{3.2}$$

$$\eta(H) = 0, \tag{3.3}$$

where U, the value of the upstream velocity, is assumed to be known. The solution of this problem would correspond to the solution of the DJL equation over a long flat central portion of the topography where $\eta_{xx} \approx 0$. The two-point boundary-value problem is easily solved with a shooting method (note that the auxiliary condition required for the conjugate flow eigenvalue problem is no longer necessary, and indeed when topography is included, momentum flux is no longer conserved). As is evident from figure 8, the solution yields an excellent estimate for the wave-induced velocities at the crest of the large trapped disturbance, even for topography that has no flat central portion. The accuracy of the estimate decreases with increasing topographic amplitude, however, even for the case corresponding to figure 7(*e*), the theory accurately predicted the disturbance-induced currents over the majority of the water column. As $U \longrightarrow \infty$, the stratification term in (3.1) drops out and the isopycnal displacement is linear, with the maximum absolute value at the bottom, in agreement with potential flow theory. The two-layer problem corresponding to (3.1) is easily derived and leads to a fifth-order polynomial equation and will be discussed in the following section on two-layer theory.

We have subjected the trapped disturbances to two types of perturbation. In the first series of simulations, the far-upstream density field was perturbed by a small-amplitude modulated superposition of wave disturbances. The resulting wave packet was allowed to advect into the trapped disturbance. While some growth of the wave packets, and even small overturns, occurred during the interaction with the large trapped disturbance, the trapped disturbance remained essentially unchanged after the interaction was complete. This result is not unexpected, as the

background current is supercritical to all linear vertically trapped waves and ISWs of all amplitudes. A second type of perturbation we investigated consists of a slowly slackening background current, so that after a set period of time $U < c_j$. It is possible that a slackening of the background current could produce upstream propagating ISWs in an efficient manner. However, in the majority of our simulations, the fluid response was dominated by steepening, and eventually a massive overturning of the downstream face of the trapped disturbance. A three-dimensional model is required to study this problem further, and in particular to quantify the considerable irreversible mixing (Caulfield & Peltier 2000; Peltier & Caulfield 2003) over, and downstream of, the topography.

4. Comparison with two-layer flows

The literature on the flow of a two-layer fluid over topography is extensive, though a good overview can be obtained from the monograph by Baines (1995), especially chapter 3. Baines discusses experimental results and suggests that many of the qualitative aspects of the experiments can be predicted on the basis of the eKdV equation. As mentioned in § 1, the solitary wave solutions of the eKdV equation are bounded above by the limit of flat-centred waves, in contrast to the solitary wave solutions of the KdV equation which are bounded above by wave breaking. However, while the eKdV includes both quadratic and cubic nonlinear terms, it is formally not a higher-order theory than that leading to the KdV equation, since both keep only the first-order dispersive term. An examination of figure 3.19 of Baines (1995), which shows the numerical integration of a forced eKdV equation in different parameter regimes, as originally published in Melville & Helfrich (1987), reveals a considerable qualitative similarity to the results of § 3. One notable difference is the small size of the trapped disturbance for the supercritical case in figure 3.19 of Baines (1995). As the solitary wave solutions of the eKdV equation have a limiting amplitude (Baines 1995, equation 3.7.11) it seems reasonable to compare this limiting behaviour to the fully nonlinear solitary wave amplitude in a two-layer fluid. The latter corresponds to the conjugate flow, as in the continuously stratified case. Under the Boussinesq approximation, the solutions for the conjugate flow amplitude for the two-layer case indicate that the displaced interface is found at the mid-depth and the propagation speed of the disturbance is independent of the initial interface position (Lamb 2000, equations 31 and 32, which match the expressions derived in Amick & Turner 1986). In figure 9, we compare the conjugate flow amplitudes to the predictions from eKdV theory and find that Baines' assertion (Baines 1995, p. 129) that the eKdV theory is appropriate for interfaces found between $z = 0.35H$ and $0.65H$ of the total depth, with rapid decay of validity outside of this range, is correct. Note, that this implies that for the results discussed in § 3, the eKdV, in pointed contrast to conjugate flow theory and its extension discussed above, does not provide an accurate predictive tool for the large-amplitude responses found over, and upstream of, the topography. Indeed, amplitudes of the actual response are more than double the size of the maximal response predicted by eKdV theory for 'dissipationless bores' (or 'inviscid bores' in Baines' terminology) with an even larger discrepancy for the large trapped disturbances.

A two-layer analogue for the theoretical description of the vertical structure at the crest of the trapped disturbance, (3.1)–(3.3), can be derived by applying the arguments found in Lamb (2000), making the Boussinesq approximation (with a reference density ρ_0) for simplicity. Consider an upstream state characterized by a

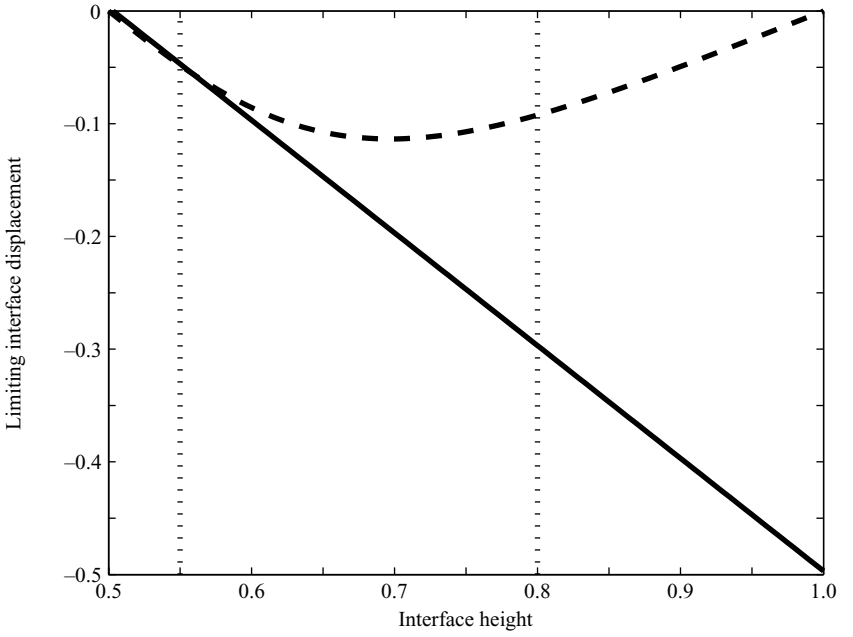

FIGURE 9. Maximal isopycnal displacement for two-layer flow under the Boussinesq approximation as a function of undisturbed interface height. —, conjugate flow theory; - - -, eKdV theory.

constant inflow velocity U, depth H, lower-layer thickness h_1, lower (upper)-layer density ρ_1 (ρ_2). The downstream state has a total depth $H+h$, lower-layer depth $h_1^* = h_1 + b$, and lower (upper)-level velocity U_1 (U_2). Two algebraic equations can be found by demanding conservation of volume flux for each of the two layers, and a third can be derived by writing down Bernoulli's theorem for a streamline along the surface and the bottom, then taking the difference between the two expressions (see Lamb 2000 for details). The three equations for the three unknowns (b, U_1, U_2) in terms of the parameters defined above and with the two additional parameters

$$N_1^2 = (\rho_1 - \rho_2)g, \tag{4.1}$$

$$\gamma = g\rho_2, \tag{4.2}$$

defined for convenience (as in the continuously stratified case we have absorbed ρ_0), read

$$Uh_1 = U_1(h_1 + b), \tag{4.3}$$

$$U(H - h_1) = U_2(H + h - h_1 - b), \tag{4.4}$$

$$0 = \tfrac{1}{2}U^2\left[\frac{(H-h_1)^2}{(H+h-h_1-b)^2} - \frac{h_1^2}{(h_1+b)^2}\right] - \gamma h - N_1^2 b. \tag{4.5}$$

These may be reduced to a single fifth-order polynomial equation in b. However, this equation does not allow an analytical solution, though it is readily solved numerically. In order to be physically relevant, solutions must satisfy $0 < h_1 + b < H + h$. In figure 10, we show the computed layer thicknesses as a function of the inflow velocity (scaled by the conjugate flow speed) for parameters corresponding to the

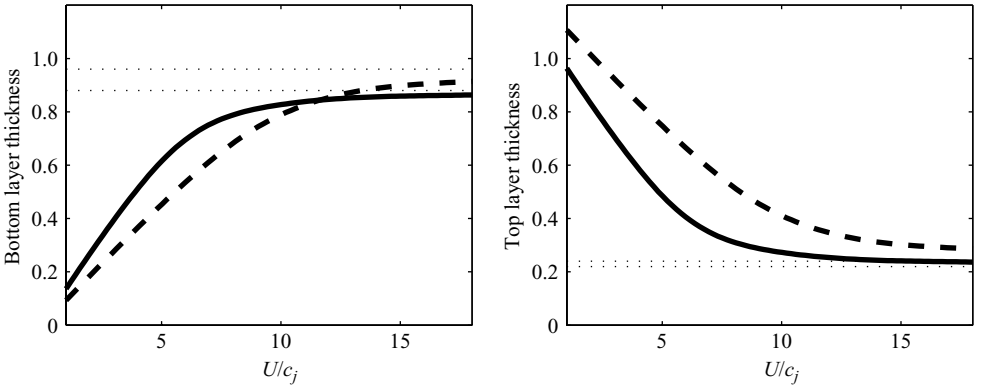

FIGURE 10. Layer thicknesses (normalized by the upstream depth H) for the two-layer version of the problem given by (3.1), (3.2) and (3.3) as functions of the inflow velocity (normalized by the conjugate flow speed c_j). Results for two different topography amplitudes are shown (—, $h = -0.1$; - - -, $a = -0.2$). The $U \longrightarrow \infty$ limit is indicated by dotted lines.

disturbance over the mid-point of the depression in the simulations of the previous section. It is clear that the range of inflow speeds for which the trapped disturbance has a large amplitude increases significantly as the topography amplitude increases. For isolated topography, such as (2.24), this implies that the theory developed in the present article will provide a good approximation when U is near c_j. As U increases and the amplitude of the trapped disturbance decreases, the η_{xx} term in the DJL equation, which is largely determined by the topography for the trapped disturbances, will become increasingly important when compared with the η_{zz} term, thereby invalidating the approximation made in applying the theory.

Another aspect of WNL theory, namely the predicted range of inflow speeds for which resonant generation is efficient in producing an upstream response, may be tested within the two-layer setting. The WNL estimate we employ is that given by equations (7.4*a*) and (7.4*b*) of Grimshaw & Smyth (1986) which are a form of their hydraulic theory-based estimate (7.1) specialized to two-layer flow. However, since (7.4*a*) and (7.4*b*) of Grimshaw & Smyth (1986) are set up to discuss a laboratory experiment in which the topography is a towed obstacle near the surface, the formulae (Grimshaw & Smyth's d, in particular) have been modified for the present situation. In figure 11, we show the predicted range of inflow speeds along with the linear long-wave speed and the (constant) conjugate flow speed as functions of the undisturbed interface height. We non-dimensionalize the velocities by the mode-1 linear long-wave speed for the two-layer case in which the interface is at the mid-depth. The amplitude of the topography is $h = -0.1$. From the figure, we see that the upper bound predicted by WNL exceeds the conjugate flow speed for interface heights between the mid-point and about 0.83. For interface heights above 0.85, the WNL upper bound is significantly lower than the conjugate flow speed, and the upper bound on the range of inflow speeds is underestimated. In figure 11, we have also included the range of inflow speeds that yielded upstream-propagating ISWs for the continuously stratified case discussed in § 3 with $(z_0, d) = (0.8, 0.05)$. For this case, the two-layer WNL upper bound is reasonable (an error of approximately 10 %), though for an arbitrary stratification it is unclear where the WNL upper bound curve crosses the curve of conjugate flow speeds.

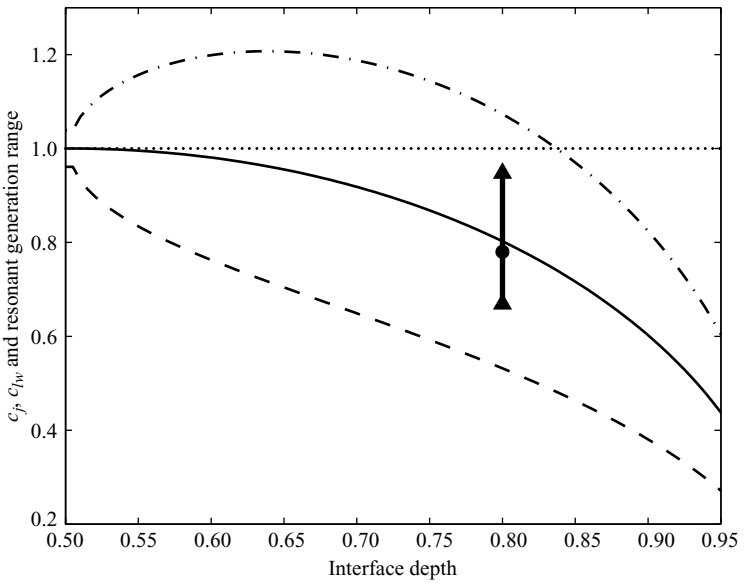

FIGURE 11. —, the linear long-wave speed; . . ., the (constant) conjugate flow speed, and the range of inflow speeds U predicted by fKdV theory to yield efficient resonant generation of upstream propagating ISWs (– · –, upper bound; - - -, lower bound), as functions of interface height. The mode-1 linear long-wave speed for the continuously stratified case discussed $(z_0, d) = (0.8, 0.05)$ is indicated by a circle. The actual range over which resonant generation efficiently generates upstream propagating ISWs is given by the vertical solid line terminated by triangles.

Figure 11 shows no major systematic error for the lower bound predicted by WNL (as it does for the upper bound). However, for low inflow speeds the upstream response consists of many linear waves along with very small ISWs, making it difficult to pick a precise point below which we can say the numerical simulations yield no upstream propagating ISWs.

The two-layer results, and the inaccuracies of the WNL theories in this context, are consistent with attempts to use the eKdV equation to model large-amplitude ISWs in a continuously stratified fluid (K. G. Lamb, personal communication). The failure of WNL theory to provide a good upper bound on inflow speeds for resonant generation stems from a failure to include 'all the nonlinearity' that governs fully nonlinear ISWs. In contrast, the conjugate flow solution, which makes no approximation of the nonlinearity governing the ISWs, but neglects dispersion in its entirety, provides an excellent upper bound. As discussed above, the lower bound is considerably more subjective and the applicability of the WNL estimate of it will probably depend on any given application or experimental set-up. A particular concern is that the amplitude of the topography can be expected to play a significant role in setting the lower bound. For example, with $U = 0.9$, close to the lowest U for which a clear upstream propagating wavetrain is produced when $h = -0.1$, we found that increasing the topographic amplitude led to a rapid increase in the amplitude of the leading upstream-propagating ISW ($h = -0.1$, -0.15 and -0.2 yields $\eta_{max} \approx 0.03$, 0.08 and 0.11).

The two-layer situation provides insight into the behaviour on the downstream side of the topography. In particular, the numerical solutions of the eKdV equation shown in the middle panel of figure 3.19 of Baines (1995) have a downstream

response not unlike figures 3 and 4 of the present study, though the amplitude, and possible instability (see figure 3) of the downstream response cannot be described by the eKdV equation. The importance of shear instability and subsequent turbulent breakdown is apparent in figures 3.17 (bottom panel) and 3.21 of Baines (1995) (much more clearly in the latter), which show several experimental realizations of what Baines and Lawrence (Baines 1995, p. 133) refer to as a 'supercritical leap'. All three experimental realizations exhibit turbulent behaviour, and hence it is premature to make a comparison with the two-dimensional simulations reported on in this investigation. However, we do note that a suite of simulations performed with $(z_0, d) = (0.8, 0.03)$ led, not unexpectedly, to a greater incidence of shear instability in the downstream response. Thus, by choosing a more diffuse pycnocline it is possible to stabilize the downstream response while maintaining the qualitative characteristics (the 'supercritical leap') of the experiments. Indeed, in figure 3 of this investigation, the instability does not set in over the topography as in the experiments. The large-amplitude downstream response merits detailed future investigation, though a three-dimensional model will probably be required in order to explore the portions of parameter space in which turbulence is important.

5. Generation of mode-2 waves

The results of § 3 leave little doubt as to the efficiency of the resonant generation mechanism for generating mode-1 waves. Moreover, a variety of theoretical tools are available for the description of mode-1 waves generated both upstream and downstream of the topography. This theoretical support structure is, in large part, not applicable to higher mode waves. Considering mode-2 waves in particular, this is because shorter mode-1 waves may propagate at the same speed as the mode-2 finite-amplitude wave, and thus can drain energy from any would-be solitary wave. Notice that this precludes an application of the variational formulation for mode-2 waves. A typical experimental set-up for generating mode-2 waves consists of a region of intermediate density fluid that is suddenly allowed to collapse by the rapid removal of a barrier. The collapse leads to the formation of a gravity current in the, generally sharp, pycnocline. For appropriate choices of parameters (intermediate density fluid volume, pycnocline thickness, maximum buoyancy frequency in the pycnocline, etc.) mode-2 waves propagate upstream faster than the gravity current. The efficacy of this generating mechanism can be understood as being due to the fact that a projection of the initial perturbation onto the linear long-wave modes (which are complete, Yih 1965) will deliver the largest amplitude at mode-2.

The resonant generation mechanism for isolated bell-shaped topography does not necessarily deliver a perturbation with the largest component at mode-2. Still, we have found that it is possible to generate mode-2 waves resonantly. Figure 12 shows the evolution of a mode-2 solitary-like wave for a stratification with $z_0 = 0.55$ and the forcing parameters $(U, h, a) = (0.275, 0.1, 1)$, note $U = 1.04c_{lw}^{(2)}$. The wave-induced horizontal velocities are shaded (values indicated by the bar) and density contours are indicated by black lines. Figure 12(a) shows the mode-2 wave at $t = 10.7$. It can be seen that despite its relatively small size, $\eta_{max} \approx 0.08$, the mode-2 wave is breaking. Moreover, the breaking region is preferentially found below the centre of the undisturbed pycnocline. A small-amplitude tail is barely visible, trailing behind the mode-2 wave. In figure 12(b), we show the mode-2 wave at $t = 17.8$. At this point in time, the leading mode-2 wave is approaching the topography crest. The breaking region now extends some distance behind and below the main wave. A mode-1 tail

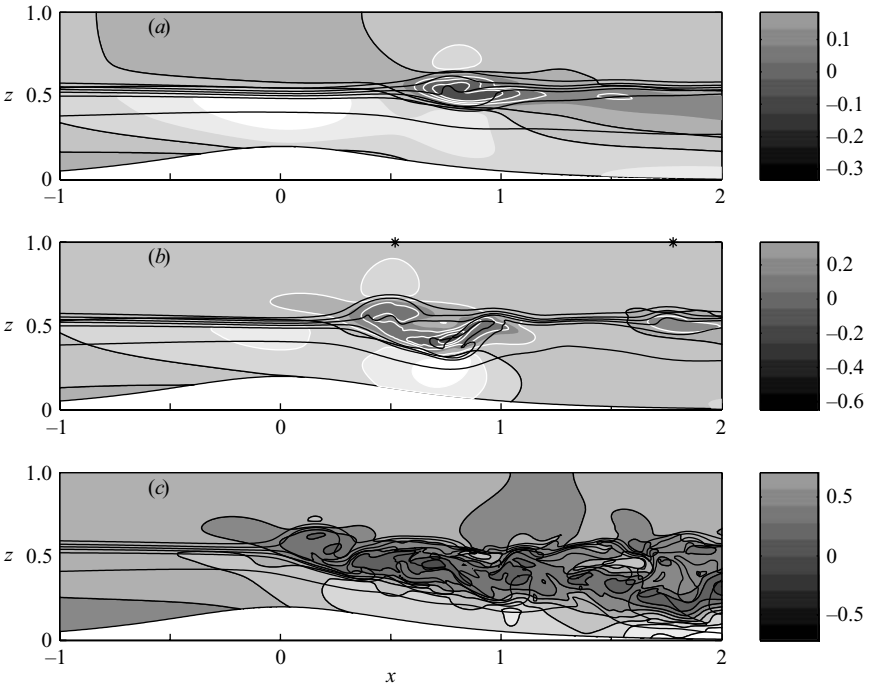

FIGURE 12. Shaded wave-induced horizontal velocities with superimposed black density contour lines for the evolution of a resonantly generated mode-2 solitary-like wave. $(U, h, a) = (0.275, 0.1, 1)$. (*a*) $t = 10.7$, (*b*) $t = 17.8$ the location of the crest for each of the two waves is indicated by an asterisk at the top boundary, (*c*) $t = 28.5$.

is clearly visible behind the leading wave. The mode-1 tail is terminated by a second smaller-amplitude mode-2 wave. The approximate crests of each of the two mode-2 waves are indicated by an asterisk at $z = 1$. Subsequent evolution is dominated by the extension of the breaking region farther downstream of the leading mode-2 wave. This is shown at $t = 28.5$ in figure 12(*c*). The second mode-2 solitary-like wave has been consumed by the downstream extension of the breaking region. The breaking region consists of Kelvin–Helmholtz-like billows that originate in the leading mode-2 wave and propagate down the topography slope. The similarity with simulations of pulsating downslope windstorms (Scinocca & Peltier 1989) is striking. While care must certainly be exercised in interpreting the flow delivered by a two-dimensional numerical model, it seems obvious that, in the present case, the importance of wave-breaking and the resulting downslope vortex shedding far outweighs wave damping due to a small-amplitude mode-1 tail.

A fair question to ask at this point is whether these results could have been predicted *a priori*. If we consider the weakly nonlinear expression for the ISW propagation speed (2.14), we note immediately that the changes in propagation speed are determined entirely by the magnitude of the nonlinear coefficient r_{10} for a given mode. Thus, according to KdV theory, a larger value of r_{10} allows a larger range of ISW amplitudes (recall that KdV theory predicts that ISW amplitude is always limited by wave breaking), and thus presumably a larger range of inflow velocities for which ISWs are generated. For example,

$$\eta_j(z_0 = 0.55) = 0.14\eta_j(z_0 = 0.80),$$

while

$$r_{10}^{(1)}(z_0 = 0.55) = 0.11 r_{10}^{(1)}(z_0 = 0.80),$$

a very reasonable level of agreement (the superscripts denote mode number). With $z_0 = 0.55$, mode-2 waves are breaking limited, however,

$$r_{10}^{(2)}(z_0 = 0.55) = 1.06 r_{10}^{(1)}(z_0 = 0.80)$$

and

$$r_{10}^{(1)}(z_0 = 0.55) = 0.1 r_{10}^{(2)}(z_0 = 0.55),$$

and thus mode-2 waves can be reasonably expected as the result of flow over topography for a significant range of inflow velocities. In contrast, we find

$$r_{10}^{(1)}(z_0 = 0.80) = 7.0 r_{10}^{(2)}(z_0 = 0.80),$$

and thus we do not expect mode-2 solitary-like waves to be generated in an efficient manner when $z_0 = 0.8$. This has been confirmed by the numerical simulations.

For a given stratification and background velocity profile it is computationally inexpensive to compute $r_{10}^{(1)}$ and $r_{10}^{(2)}$. The ratio of the two gives a simple and rough assessment of whether resonant generation of mode-2 solitary-like waves can reasonably be expected. This is useful for situations in which the background current increases slowly, such as the semidiurnal tide in fjords, passing through the mode-2 linear long-wave speed first and exceeding the mode-1 linear long-wave speed only a considerable length of time (of the order of an hour) later. Comparing the present criterion with equation (7.1) of Grimshaw & Smyth (1986), we find that in our criterion we are neglecting the role of hill amplitude. Given the rather poor upper bound on the range of inflow speeds that the WNL criterion of Grimshaw & Smyth yields in the two-layer case with topography of moderate amplitude ($h = -0.1$), as discussed in § 4, this seems a reasonable alternative. It should be noted that we employ WNL as a proxy for fully nonlinear solutions of the DJL equation (especially the mode-2 solutions which cannot be found by the variational technique we employ), as opposed to a stand-alone theory. In the future, it would be desirable to construct a reliable numerical solver for the higher-mode solutions of the DJL equation, though the problem of fully nonlinear mode-2 waves with mode-1 tails is numerically non-trivial, as discussed in Rusas & Grue (2002) in the context of three-layer fluids.

We have found that with negative topography, it is possible to generate trapped mode-2 disturbances over the topography that match mode-2 solutions to the boundary-value problem, (3.1)–(3.3). This is interesting in itself since for the stratification employed, mode-2 waves are breaking limited and thus there is no *a priori* known value of U above which no upstream propagating mode-2 disturbances are possible (though see Lamb & Wilkie (2004) for an extension of the conjugate flow concept to waves with trapped cores that is successful in describing breaking waves in some circumstances). However, the mode-2 trapped disturbances we have found are considerably smaller in amplitude than their mode-1 counterparts. We note that it would certainly be possible to construct a model stratification which allows for large-amplitude non-breaking mode-2 trapped disturbances and that does not explicitly preclude mode-1 waves, though it is unclear whether such a stratification would have any relevance for studies of the coastal ocean. An alternative avenue for future work would attempt to mimic numerically the experimental set-up employed by Mehta *et al.* (2002) to generate resonantly mode-2 solitary waves with radiating tails by gravity currents that intrude into a layered fluid.

6. Discussion

Taken as a whole, the simulations discussed in the previous sections demonstrate that the resonant generation mechanism for ISWs is extremely robust. As mentioned in § 1, the literature on resonant generation is heavily slanted toward weakly nonlinear theory. This implies that for the case of small-amplitude topography, the amplitude of the resonantly generated waves is expected to exceed the amplitude of the topography itself, but no predictions as to the limiting ISW amplitude and the nature of the upper bound can be given. Fully nonlinear theory based on the DJL equation does allow the calculation and classification of the upper bound on ISW amplitude and we have chosen to concentrate on situations for which the ISW amplitude is bounded above by the conjugate flow amplitude (the limit of flat-centred waves). This allowed us to compare with the particularly simple conjugate flow theory for two-layer fluids as well as the weakly nonlinear theory based on the eKdV equation that has been used to interpret experiments in the past (Baines 1995). We found that conjugate flows for the continuously stratified case match the limiting upstream propagating waveform (a 'dissipationless bore') and that the two-layer conjugate flows are reasonable approximations of the continuously stratified case. The weakly nonlinear theory (eKdV), however, underpredicts the amplitude of the limiting waveform, for our choice of stratification by more than 50 % of the actual value. The two-layer situation was employed to demonstrate that weakly nonlinear theory (based on the fKdV equation) incorrectly predicts the upper bound on the range of inflow velocities for which a significant upstream response is obtained. In particular, in a two-layer situation, the WNL theory underpredicts the true upper bound for some interface heights and overpredicts for others. The conjugate flow theory, on the other hand, provides the correct upper bound in all cases considered. The lower bound given by WNL is much more reasonable, though the issue is confounded by the sensitivity of the amplitude of the resonantly generated upstream-propagating ISWs to the topography amplitude. Thus, for small waves, a precise cutoff below which 'no upstream propagating ISWs are generated' is subjective. Nevertheless, the present results suggest that the WNL estimate of the lower bound is reasonable.

The weaknesses of WNL described above are consistent with past attempts at comparing weakly nonlinear theory and fully nonlinear waves. Lamb & Yan (1996) compared weakly nonlinear descriptions of an undular bore with time-dependent integrations of the full Euler equations (under the Boussinesq approximation). They found that first-order theory improves upon leading-order theory, but its use to describe finite-amplitude waves requires subjectively choosing several undetermined constants (see Lamb & Yan 1996 for details). Perhaps more to the point, Lamb (1999) found that in describing ISWs near the limiting amplitude, the choice of vertical coordinate (the Eulerian z employed in the present paper, or the upstream isopycnal height $y = z - \eta(x, z)$ sometimes referred to as Euler–Lagrange theory) profoundly influences the accuracy of the weakly nonlinear theory. Moreover, Lamb (1999) demonstrated that Eulerian weakly nonlinear theory produces better results for the widely used exponential density profile, while Euler–Lagrange weakly nonlinear theory produces better results for a single pycnocline stratification, such as that used in this study. This implies that instances in which choosing the appropriate vertical coordinate improves the fit of theory with oceanic measurements, as in Trevorrow (1998), are not general. Indeed, given that it is numerically inexpensive to solve the DJL equation for a given stratification, it is perhaps best to use WNL as a qualitative as opposed to a quantitative tool.

The conjugate flow theory succeeds in describing both the propagation speed and the vertical structure of the limiting ISW, essentially exactly. More importantly, the observation that no upstream propagating ISWs are possible for inflow speeds above the conjugate flow speed, c_j, led us to investigate the fluid response for inflow speeds slightly larger than c_j. We found that for a band of inflow velocities above c_j, large disturbances form, and remain trapped, over the topography. The shape of these disturbances is essentially specified by the topography (and thus for isolated topography the disturbances resemble ISWs). However, the amplitude of the disturbances can reach 200 % of the limiting ISW amplitude. Despite their large amplitude, these disturbances remain laminar and proved stable under a variety of upstream introduced perturbations. Indeed, the large trapped disturbances are solutions of the DJL equation with c specified to cancel the upstream velocity, and the isopycnal displacement at the bottom chosen to match the topography. As such, it is possible to construct a theory for the structure at the crest of the trapped disturbances by neglecting isopycnal curvature (the η_{xx} term in the DJL equation). This theory is similar in structure to the conjugate flow theory, but momentum flux is no longer conserved. We found that the theory provides excellent (and computationally inexpensive) estimates for properties at the crest of the largest trapped disturbances, with a decrease in accuracy as the inflow speed increases and the trapped disturbance amplitude decreases. We constructed a two-layer analogue of the continuously stratified theory and used it to show that the range of inflow speeds for which large trapped disturbances are formed increases rapidly with increasing topography amplitude.

For a situation in which the inflow speed changes in time, the large trapped disturbances provide a possible source for a substantial amount of irreversible mixing. Indeed, a current that slackens from a value greater than c_j to one less than c_j will generally lead to large-scale overturning events over the topography as the large trapped disturbance breaks up. The investigation of these breaking events will require three-dimensional computations and provides a clear direction for future work.

As the weakly nonlinear theory of resonant generation makes no distinction between mode-1 and higher-mode waves, we attempted to generate mode-2 solitary-like waves resonantly. For stratifications with a main pycnocline near (but not at) the mid-depth, the generation proceeded much as for mode-1 waves. In agreement with theory, the mode-2 waves were trailed by a small-amplitude mode-1 tail. It is this tail that precludes true mode-2 solitary waves. However, we found that for a single pycnocline stratification, mode-2 waves were breaking for all but the smallest amplitudes, and that it is the wave-breaking and not the mode-1 tail that dominates energy dissipation and wave decay. In contrast to previous literature on mode-2 waves that computed mode-1 waves and reflected about a line of symmetry to produce mode-2 waves (Tung *et al.* 1982; Terez & Knio 1998), we have found that mode-2 solitary-like waves are highly asymmetric in the vertical.

The results discussed in this paper are more relevant to a laboratory setting (i.e. an obstacle is suddenly accelerated in still stratified fluid) than an oceanic situation, because the 'forcing' in the coastal ocean is dominated by the barotropic tide. Nevertheless, in our previous work on tidally generated ISWs over the sill at Knight Inlet (Stastna & Peltier 2004), we found that the impulsively started simulations provided insight into the considerably more complex simulations of the time varying tidal forcing. Furthermore, there are reported instances of resonant generation in the ocean (see Bogucki *et al.* 1997; Wang & Redekopp 2001 for discussion), and these provide a rich source of problems for future investigation.

An important issue relevant to the laboratory scale that remains for future investigation is whether either three-dimensional or viscous effects can destabilize the large trapped disturbances. We plan to examine these issue using numerical simulations in the near future. While the transient portion of the impulsively started simulations is of most potential interest to experimentalists (who cannot tow an obstacle past the upstream wall of the tank), the long-term evolution of the simulations is of obvious theoretical interest, and serves as another potential avenue for future investigation. Of particular interest are the existence and characteristics of any limit cycles as the inflow speed and topography amplitude are varied.

We gratefully acknowledge useful discussions with Kevin Lamb and Dick Lindzen. This work was supported by the Natural Sciences and Engineering Research Council (NSERC) of Canada through NSERC grant A9627. The comments of three anonymous referees and the editor led to a significantly improved paper and are gratefully acknowledged.

REFERENCES

Akylas, T. R. & Grimshaw, R. H. J. 1992 Solitary internal waves with oscillatory tails. *J. Fluid Mech.* **242**, 279–298.

Amick, C. J. & Turner, R. E. L. 1986 A global theory of internal solitary waves in two-fluid systems. *Trans. Am. Math. Soc.* **298**, 431–452.

Apel, J. R., Holbrook, J. R., Liu, A. K. & Tsai, J. J. 1985 The Sulu Sea internal soliton experiment. *J. Phys. Oceanogr.* **15**, 1625–1651.

Baines, P. G. 1995 *Topographic Effects in Stratified Fluids*. Cambridge University Press.

Bell, J. B. & Marcus, D. L. 1992 A second-order projection method for variable-density flows. *J. Comput. Phys.* **101**, 334–348.

Benney, D. J. 1966 Long nonlinear waves in fluid flows. *J. Math. Phys.* **45**, 52–69.

Bogucki, D., Dickey, T. & Redekopp, L. G. 1997 Sediment resuspension and mixing by resonantly generated internal solitary waves. *J. Phys. Oceanogr.* **27**, 1181–1203.

Caulfield, C. P. & Peltier, W. R. 2000 The anatomy of the mixing transition in homogeneous and stratified free shear layers. *J. Fluid Mech.* **413**, 1–47.

Cummins, P. F., Vagle, S., Armi, L. & Farmer, D. M. 2003 Stratified flow over topography: upstream influence and generation of nonlinear internal waves. *Proc. R. Soc. Lond.* A **459**, 1467–1487.

Davis, R. E. & Acrivos, A. 1967 Solitary internal waves in deep water. *J. Fluid Mech.* **29**, 593–607.

Grimshaw, R. & Smyth, N. 1986 Resonant flow of a stratified fluid over topography. *J. Fluid Mech.* **169**, 429–464.

Grimshaw, R. H. J. & Zengxin, Y. 1991 Resonant generation of finite amplitude waves by the flow of a uniformly stratified fluid over topography. *J. Fluid Mech.* **229**, 603–628.

Grue, J., Jensen, A., Rusas, P. O. & Sveen, J. K. 2000 Breaking and broadening of internal solitary waves. *J. Fluid Mech.* **413**, 181–217.

Lamb, K. G. 1994 Numerical simulations of stratified inviscid flow over a smooth obstacle. *J. Fluid Mech.* **260**, 1–22.

Lamb, K. G. 1997 Are internal solitary waves solitons? *Stud. Appl. Maths* **101**, 289–309.

Lamb, K. G. 1999 Theoretical descriptions of shallow-water solitary internal waves: comparisons with fully nonlinear waves. *The 1998 WHOI/IOSA/ONR Internal Solitary Wave Workshop: Contributed Papers, Woods Hole Oceanographic Institution Tech. Rep.* (ed. T. F. Duda & D. M. Farmer).

Lamb, K. G. 2000 Conjugate flows for a three-layer fluid. *Phys. Fluids* **12**, 2169–2185.

Lamb, K. G. & Wan, B. 1998 Conjugate flows and flat solitary waves for a continuously stratified fluid. *Phys. Fluids* **10**, 2061–2079.

Lamb, K. G. & Wilkie, K. 2004 Conjugate flows with trapped cores. *Phys. Fluids* **16**, 4685–4695.

Lamb, K. G. & Yan, L. 1996 The evolution of internal wave undular bores: comparisons of a fully nonlinear numerical model with weakly nonlinear theory. *J. Phys. Oceanogr.* **26**, 2712–2733.

Laprise, R. & Peltier, W. R. 1988 On the structural characteristics of steady finite-amplitude mountain waves over a bell-shaped topography. *J. Atmos. Sci.* **46**, 586–595.

Mehta, A. P., Sutherland, B. R. & Kyba, P. J. 2002 Interfacial gravity currents. II. Wave excitation. *Phys. Fluids* **14**, 3558–3569.

Melville, W. K. & Helfrich, K. R. 1987 Transcritical two-layer flow over topography. *J. Fluid Mech.* **178**, 31–52.

Osborne, A. R. & Burch, T. L. 1980 Internal solitons in the Andaman sea. *Science* **208**, 451–460.

Peltier, W. R. & Caulfield, C. P. 2003 Mixing efficiency in stratified shear flows. *Annu. Rev. Fluid Mech.* **35**, 135–167.

Porter, A. & Smyth, N. F. 2002 Modelling the morning glory of the Gulf of Carpentria. *J. Fluid Mech.* **454**, 1–20.

Rusas, P. -O. & Grue, J. 2002 Solitary waves and conjugate flows in a three-layer fluid. *Euro. J. Mech.* B. *Fluids* **21**, 185–206.

Schmidt, N. P. & Spigel, R. H. 2000 Second mode internal solitary waves II – Internal circulation. In *Fifth Intl Symp. on Stratified Flows* (ed. G. A. Lawrence, R. Pieters & N. Yonemitsu), pp. 815–820.

Scinocca, J. F. & Peltier, W. R. 1989 Pulsating downslope windstorms. *J. Atmos. Sci.* **46**, 2885–2914.

Stamp, A. P. & Jacka, M. 1996 Deep-water internal solitary waves. *J. Fluid Mech.* **305**, 347–371.

Stastna, M. & Lamb, K. G. 2002 Large fully nonlinear internal solitary waves: the effect of background current. *Phys. Fluids* **14**, 2987–2999.

Stastna, M. & Peltier, W. R. 2004 Upstream propagating solitary waves and forced internal wave breaking in stratified flow over a sill. *Proc. R. Soc.* A **460**, 3159–3190.

Terez, D. E. & Knio, O. M. 1998 Numerical simulations of large-amplitude internal solitary waves. *J. Fluid Mech.* **362**, 1–44.

Trevorrow, M. V. 1998 Observations of internal solitary waves near the Oregon coast with an inverted echo sounder. *J. Geophys. Res.* **103**(C4), 7671–7694.

Tung, K. K., Chan, T. F. & Kubota, T. 1982 Large amplitude internal waves of permanent form. *Stud. Appl. Maths* **66**, 1–44.

Turkington, B., Eydeland, A. & Wang, S. 1991 A computational method for solitary internal waves in a continuously stratified fluid. *Stud. Appl. Maths* **85**, 93–127.

Wang, B. & Redekopp, L. G. 2001 Long internal waves in shear flows: topographic resonance and wave-induced global instability. *Dyn. Atmos. Oceans* **33**, 263–302.

Whitham, G. B. 1974 *Linear and Nonlinear Waves.* John Wiley.

Yih, C. 1965 *Dynamics of Nonhomogeneous Fluids.* Macmillan.